scientific reports

Check for updates

OPEN

Magnetic properties of different phases iron oxide nanoparticles prepared by micro emulsion-hydrothermal method

Shakeel Ahmad[1], Henmei Ni[1]✉, Fahad S Al-Mubaddel[2], Moustafa A. Rizk[3,4], Mohamed Ben Ammar[5], Afaq Ullah Khan[6], Zainab M. Almarhoon[7], Abdulaziz A. Alanazi[8] & Magdi E. A. Zaki[9]✉

In this study, we report the synthesis of iron oxide nanoparticles (FeONPs) using micro-emulsion-hydrothermal method. By adjusting the synthesis temperature, we successfully produced FeO nanorods and nanospheres. In addition, the 2-octanol, and the surfactant cetyltrimethylammonium bromide served as a solvent in the synthesis process. Using iron nitrate hexahydrate as the salt precursor allowed for the formation of FeONPs with varied sizes, shapes and phases. The synthesized materials were extensively characterized using XRD, SEM, TEM, EDS, FTIR, and XPS techniques. However, the structural analysis revealed rhombohedral (hematite), and (magnetite) crystal structures in the materials synthesized at different temperature and durations, with particles ranged in size from 12 to 97 nm. More importantly, the magnetic characterization, performed with a vibrating sample magnetometer and SQUID magnetometer, indicated that the NPs showed not clear superparamagnetic behavior. In conclusion, this work demonstrates the synthesis of FeONPs with controlled size, shape and phase using microemulsion hydrothermal technique, with detailed characterization offering valuable insights into their magnetic and structural properties.

Keywords FeONPs, Microemulsion-hydrothermal method, Magnetic properties

In recent decades, nanotechnology has garnered significant interest across various research fields, aiming to develop nanoscale materials through different techniques, including physical and chemical methods. Nanoparticles, with diameters ranging from 1 to 100 nm, possess unique and controllable properties distinct from their bulk counterparts[1,2]. The Materials comprising nanoparticles, nanotubes, and nanofibers demonstrate a wide range of electrical, magnetic, electro-optical, and chemical properties[3,4]. Notably, nanoparticles exhibit specific behaviors attributed to the high fraction of atoms residing on their surfaces and the finite number of atoms within each crystalline core. Initially observed in magnetic materials[5], these finite-size effects have also been identified in nonmagnetic materials such as semiconductors[6,7]. Wide-ranging applications of FeONPs in biology, electronics, and industry are well known. Compared to conventional micrometer-sized particles, these particles, measuring in size from 1 to 100 nanometers (nm), exhibit greater attributes[8]. The synthesis of magnetic nanoparticles is achieved by a range of methods, such as mechanical powder breakdown[9], the Massart process, specific precipitation techniques[10], impregnation[11], and sol-gel preparation[12]. Lauric acid is also used as a non-aqueous medium[13]. The method of choice is determined by several variables, including the required particle size, characteristics, scalability, and resource availability. Among these approaches, the microemulsion method has gained significant recognition for synthesizing nanoparticles, including those with magnetic and catalytic

[1]School of Chemistry and Chemical Engineering, Southeast University, Nanjing 211189, PR China. [2]Department of Chemical Engineering, College of Engineering, King Saud University, Riyadh 11421, Saudi Arabia. [3]Chemistry Department, Faculty of Science, Suez Canal University, Ismailia, Egypt. [4]Chemistry Department, Faculty of Science and Arts (sharourah), Najran University, Najran, Saudi Arabia. [5]Center for Scientific Research and Entrepreneurship, Northern Border University, Arar 73213, Saudi Arabia. [6]School of Chemistry and Chemical Engineering, Jiangsu University, 301 Xuefu Road, Zhenjiang 212013, China. [7]Chemistry Department, College of Science, King Saud University, P.O. Box 2455, Riyadh 11451, Saudi Arabia. [8]Department of Chemistry, College of Science and Humanities in Al-Kharj, Prince Sattam bin Abdulaziz University, Al-Kharj 11942, Saudi Arabia. [9]Department of Chemistry, College of Science, Imam Mohammad Ibn Saud Islamic University (IMSIU), Riyadh 11623, Saudi Arabia. ✉email: henmei_ni@seu.edu.cn; mezaki@imamu.edu.sa

properties[14–16]. Surfactant and co-surfactant molecules stabilize the interface of microemulsions, which are stable dispersions of immiscible water and oil phases[17]. Specifically, the formation of spherical reverse micelles in the bulk oil phase is the result of the dispersion of water Nano droplets in the Water-in-Oil (W/O) microemulsion. This special system serves as a "Nano reactor" for the synthesis of nanoparticles. When two water Nano droplets collide, they combine due to Brownian motion, which promotes the exchange of reactants[18]. Since the chemical reaction is limited to the interior of the water nano droplets, the shape, size, and narrow size distribution of the particles can be controlled by varying the composition of the oil, water, and surfactant mixture using the microemulsion method[19,20]. It is important to note that the water nano domains in the microemulsion are constantly moving and crashing into one another, which facilitates inter-micellar exchange. Intermuscular exchange is highly dependent on the elasticity of the surfactant film[21]. By employing the microemulsion process and a salt precursor called $FeSO_4.nH_2O$, Antony et al.[22] investigated the magnetic characteristics of FeONPs and achieved 18 emu/g magnetic saturation. Kolic et al.[23] produced FeONPs at 30 emu/m Ms and 60Oe coercivity using the microemulsion technique and the salt $FeCl_2.7H_2O$. The magnetic characteristics of FeONPs were studied by Vidal et al.[24] using the hydrothermal process and a solution called $FeSO_4.nH_2O$ that had 108 Hc and 56 emu/g of Ms. A 37 emu/g FeONPs was produced by Chin et al.[25] using the $FeSO_4.7H_2O$ salt precursor in a microemulsion process.

We described the synthesis, morphology, structure, and magnetic characteristics of FeO nanorods, and nanospheres. In order to tune the size of magnetic FeONPs between 12 and 97 nm, which have good saturation magnetization of 213 emu/g, we modified the previous microemulsion method to a new micro emulsion-hydrothermal method. This was accomplished by employing inexpensive single-salt iron nitrate nonahydrate as a salt precursor, in the absence of any acid or base, in combination with cetyltrimethylammonium bromide as a surfactant, 2-octanol, and water as a solvent at various temperatures and times. The synthesis of FeONPs without the use of acid or base is a safer and more environmentally friendly method. These nanoparticles, synthesized without acid or base, exhibit enhanced stability and can be utilized in various applications. They have particularly important applications in medicine and environmental treatment, such as water treatment. One disadvantage of using acid or base in the synthesis process is that it introduces impurities into the final product, which can negatively impact the purity and effectiveness of the nanoparticles.

Experimental section

Materials and synthesis procedure

The chemicals such as CTAB, 2-octonal, and glycerol were acquired from Sigma Aldrich Chemical Company. Iron nitrate nonahydrate, ($Fe(NO_3)_3{\cdot}9H_2O$, $\geq 98\%$) was purchased from Sigma-Aldrich. All of the reagents were used without additional purification. The synthesis of FeONPs was conducted using the micro emulsion-hydrothermal method. To initiate the synthesis, water-in-oil microemulsions with identical compositions were prepared in separate beakers by stirring together 4.0 g CTAB, 30 mL 2-octanol, and 4 mL water for duration of one hour. The first microemulsion (referred to as microemulsion one) and the second microemulsion (referred to as microemulsion two) were based on the facts that the previous contained 8 mL glycerol and the latter one contained 0.3922 g of $Fe(NO_3)_3{\cdot}9H_2O$. Both microemulsions were stirred individually for one hour. Subsequently, microemulsion two was added to microemulsion one while continuing the stirring process. The entire reaction mixture was then stirred for an additional hour. After the completion of the one-hour stirring stage, the entire mixture was transferred to a Teflon-lined autoclave and heated at 200 °C and 400 °C temperatures for duration up to 18 h, respectively. Following the heating process, the resulting black precipitate was centrifuged at 4000 rpm for 30 min. The obtained black powder was washed multiple times with ethanol and water to eliminate any remaining oil, surfactant, and other impurities. The products obtained from reactions at different temperatures are denoted as n1 and n2, corresponding to treatments at 200 °C and 400 °C, respectively.

Results and discussion

SEM and TEM analysis

The SEM images of n2, having a size ranging from 10 nm to 97 nm are analyzed by image j software, had a characteristic rod-shaped morphology, as displayed in Fig. 1(a and b). The rods tended to group together and had smooth surfaces. The rod-shaped morphology is frequently linked to anisotropic growth and is caused by particular circumstances that existed during the synthesis process. These rods might be useful as magnetic materials or nanocomposites due to their special qualities. The TEM image of n2 depicts distinct, isolated NPs, as evidenced by the visible nanoscale rods the distribution of size and shape of the individual NPs can be better understood by TEM analysis, which offers a more in-depth look at each one, as shown in Fig. 1c. Figure 1d–f shows the spherical morphology of Fe_3O_4 NPs n1 that were synthesized at 200 °C for 18 h. These NPs exhibited sizes between 12 and 67 nm. Since spherical NPs have a high surface energy and are therefore resistant to temperature pH reaction atmosphere, and surface condition, they agglomerate. Overall, the SEM and TEM images provided a clear understanding of the surface morphology and microstructure of the synthesized α-Fe_3O_4 NPs. The various morphologies seen at various times and temperatures demonstrate how the processing parameters affect the properties of the final particles. These findings advance our knowledge of FeONPs and their possible uses in a range of industries, such as electronics, environmental remediation, and medicine.

The elemental mapping and spectrum of the α-Fe_3O_4 NPs n2 using energy-dispersive X-ray Spectroscopy (EDS) is shown in Fig. 2. The elemental composition of a sample n2 can be identified and mapped using the EDS technique. In this instance, the elemental distribution on the surface of the produced α-Fe_3O_4 NPs. is evaluated, and the purity of the particles is confirmed using EDS mapping. In particular, the rod shape of the NPs is highlighted in Fig. 2 the distribution of the elements iron (Fe) and oxygen (O) on the surface of the nanorods is depicted in these figures employing the EDS elemental mapping. The homogeneous distribution of both elements

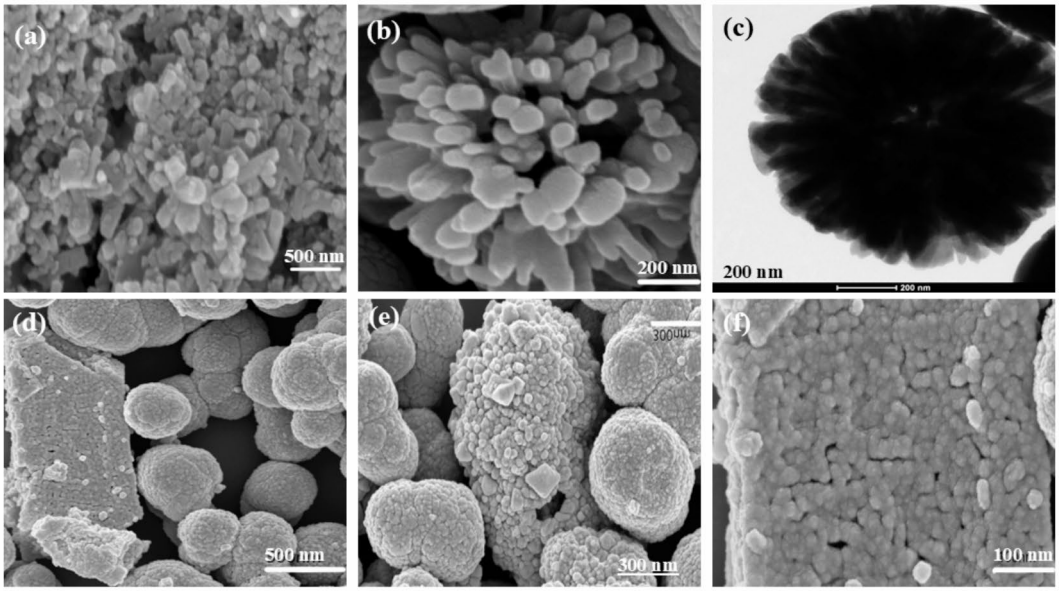

Fig. 1. SEM morphology of a FeONPs produced by a micro emulsion-hydrothermal technique. (**a**,**b**) SEM of n2, (**c**) TEM image of n2, (**d**–**f**) SEM images of n1.

in the images suggests that iron and oxygen are distributed uniformly within the NPs. This homogeneous distribution implies that the prepared NPs have a consistent elemental composition throughout their structure and indicates the presence of a well-mixed composition. Table 1 shows the FeONPs proportionate composition. The table shows that Fe makes up 76% of weight and oxygen (O) makes up 34 weight%. The stoichiometric oxygen-to-Fe ratio aligns with the composition of the as synthesized α-Fe_3O_4 NPs. This balanced indicates the successful incorporation of the desired FeO phase. Additionally, the purity and elemental distribution of the α-Fe_3O_4 NPs are strongly validated by EDS elemental mapping and composition analysis conducted in this study. These results confirm that Fe and O make up the majority of the NPs composition, where elements are evenly dispersed across the surface of the particles. Such information is valuable for understanding the chemical composition and structural characteristics of the NPs, and it supports their potential use in various applications, including catalysis, magnetic materials, and biomedical applications.

XRD analysis

The samples well-defined peaks in the X-ray diffraction (XRD) patterns, labelled as n1and n2, are displayed in Fig. 3 and suggest that the samples are crystalline in nature. The diffraction peaks observed at 2θ values of 24°, 40°, 49°, 62° and 64° correspond to the (012), (113), (024), (214) and (300) crystalline plane corresponding to hematite as referenced by [JCPDS No. 01-079-0007][26]. Additionally, peaks at 2θ values of 33°, 35°, 54° and 57° corresponding to the (200), (311), (422), and (511) planes, are attributed to the magnetite [JCPDS No. 01-076-1849][27]. This implies that the atoms in sample n1 have an uneven arrangement, crystalline structure and mixed morphologies. Meanwhile, the diffraction peaks for sample n2, appear at 2θ values of 30°, 33°, 35°, 43°, 54°, 57° and 63° are corresponding to the (200), (311), (400), (422), (511) and (440) crystalline planes, all are attributed to magnetite, as displayed in Fig. 3. This observation is further supported by the fact that increasing the synthesis temperature from 200 to 400, leads to the disappearance of hematite peaks from the XRD pattern. The precise crystal phases found in each sample are revealed by the XRD patterns, which offer insightful information. In fact, the study ensures that crystalline phases can be identified by correlating the observed peaks which specific crystallographic planes. The XRD analysis confirms the presence of hematite, maghemite, and magnetite phases in the as synthesized samples. The differences in peak sizes and shapes can also provide details about the crystal structure and crystallite size of the nanoparticles. All things considered, the XRD study and the explanation that goes with it in Table 2 offer important insights into the mixed morphologies, crystal phases, and crystallinity that the synthesized nanoparticles contain.

FTIR analysis

Based on the distinctive vibrational frequencies of particular functional groups and compounds, FTIR spectroscopy is an effective tool for locating and verifying their presence in a sample. In this instance, the formation of metal oxide nanoparticles in samples n1 and n2 is confirmed by the observed absorption peaks

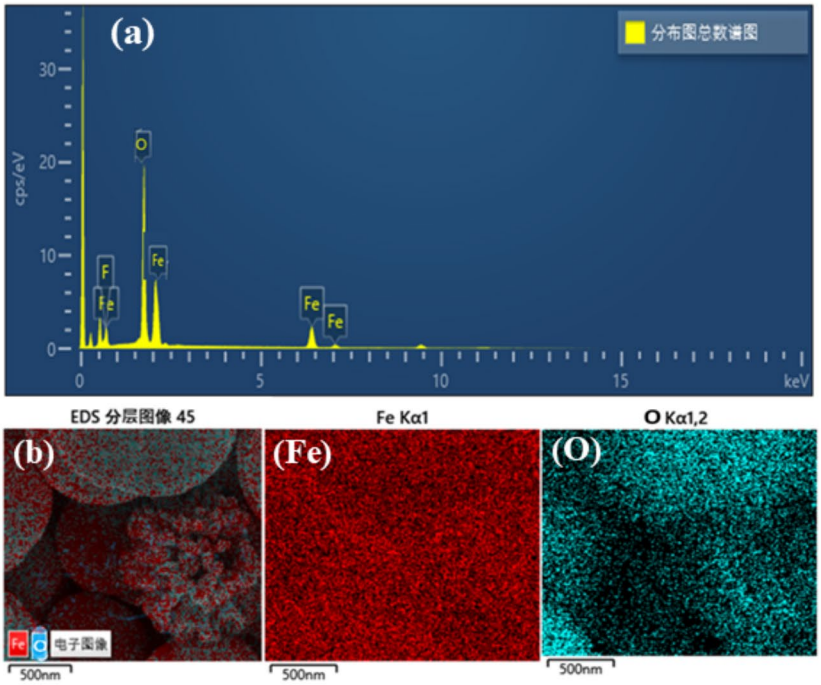

Fig. 2. (**a**) EDS analysis and (**b**) elemental mapping of α-Fe_3O_4 NPs.

Total number of distribution plot spectrum		
Elements	**Wt%**	**At%**
O	36	56.17
Fe	74	43.83
Total Amount	100.00	100.00

Table 1. The atomic weight% of α-Fe_3O_4 NPs.

at particular frequencies. The FTIR spectrum covers the range of 300–4000 cm^{-1} and provides information about the molecular vibrations and functional groups present in the samples, as displayed in Fig. 4. In the FTIR spectrum, specific absorption peaks are observed at frequencies of 384 cm^{-1}, 460 cm^{-1}, 721 cm^{-1}, 898 cm^{-1}, and 998 cm^{-1}. These peaks correspond to stretching and bending vibrations of the metal oxide nanoparticles. It is noteworthy that the observed absorption peaks are in agreement with the literature value cited as[28]. As its characteristic vibrational modes are in agreement with the published literature, this agreement implies that the synthesized samples undertaken, in particular, contain the expected metal oxide nanoparticles.

XPS analysis

X-ray Photoelectron Spectroscopy (XPS) was employed to provide further characterization of the chemical composition and bonding of the sample. Figure 5 displays the XPS spectrum, which confirms the presence of O1s and Fe2p elements. Two noticeable peaks were seen at binding energies of 711 eV and 724 eV, respectively, in the high-resolution Fe2p spectrum (Fig. 5a), which corresponds to $Fe2p_{3/2}$ and $Fe2p_{1/2}$[29]. Additionally, two satellite peaks are also observed for Fe at 719 eV and 725 eV[30], confirming the presence of iron in the sample.

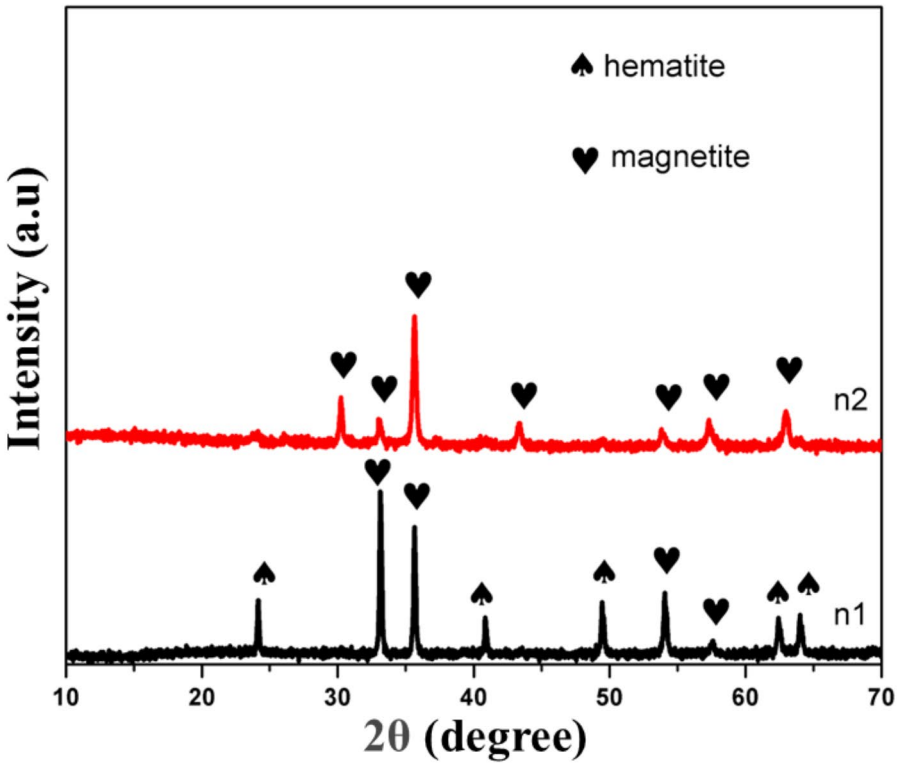

Fig. 3. XRD pattern of FeONPs prepared by microemulsion hydrothermal method at different temperatures.

Sample	Phase	Temp. (°C)	Time (h)	Crystal structure	Space group	ICDD card number	Average crystalline size (nm)
n_1	Hematite	200	30 h	Rhombohedral	p-3	01-079-0007	27
n_2	Maghemite	200	36 h	Tetragonal	P	01-076-1849	27

Table 2. XRD result of synthesis iron oxide nanoparticles by microemulsion- hydrothermal method at different temperatures and time.

Dominant oxide peaks are visible in the oxygen envelope of the XPS spectrum Fig. 5 (b) at binding energies of 530.52 eV, and 531 eV. The oxygen species found in the sample are represented by these peaks. These peaks appearance is consistent with the expected oxide characteristics[31]. The overall XPS result give the evidence that the FeONPs is successfully synthesized.

VSM analysis

The magnetic properties of the synthesized samples were studied using a Vibrating Sample Magnetometer (VSM), and their hysteresis behavior at room temperature was investigated. Based on the XRD patterns, different phases of FeO were observed in the samples. Figure 6 illustrates the characteristic hysteresis curves of the synthesized samples n1 and n2 at room temperature. These curves offer insights into the magnetic characteristics of the samples, such as saturation Magnetization (Ms), coercivity, and retentivity (Mr). Furthermore, Table 3 presents the precise values of these magnetic parameters for each sample. The Vibrating Sample Magnetometer (VSM) examination of FeONPs following distinct treatments, notably n1 treated at 200 °C and n2 treated at 400 °C, unveils fascinating magnetic attributes. Sample n1 exhibited a saturation magnetization (Ms) of 145.04 emu/gm, a retentivity (Mr) of 38.41 emu/gm, and a coercivity (Hc) of 162.83 G. In comparison, sample n2 displayed a higher saturation magnetization of 213.11 emu/gm, a retentivity of 60.98 emu/gm, and a coercivity of 173.66 G. The increase in saturation magnetization and retentivity for n2 indicates enhanced magnetic moment alignment and improved magnetic stability compared to n1. Despite the slightly higher coercivity for n2, both samples exhibit similar coercive forces, suggesting comparable resistance to demagnetization.

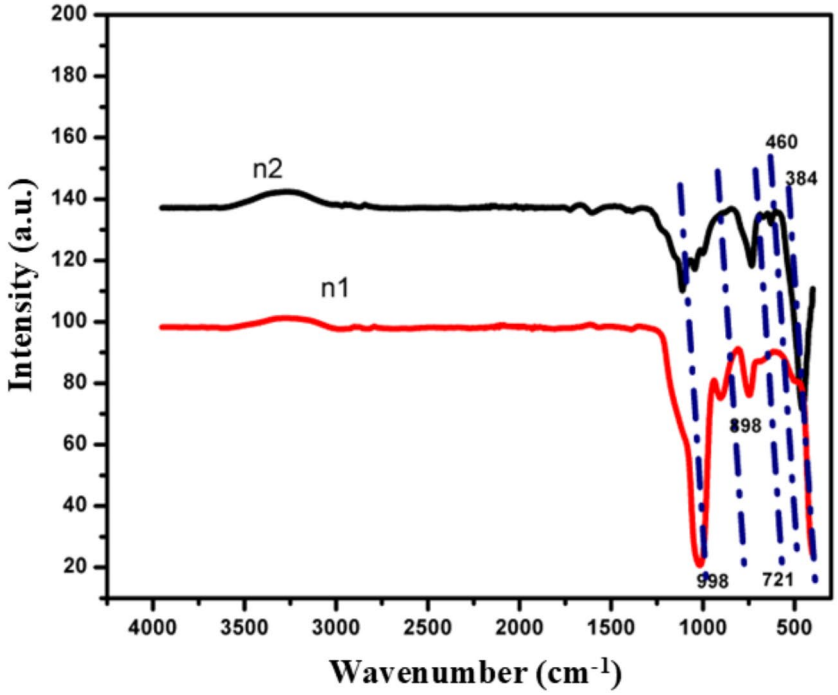

Fig. 4. The FTIR spectrum of FeONPs.

In the analysis of FeONPs samples subjected to various heat treatments, the coercivity values are pivotal in determining the weather superparamagnetic behavior is exhibited. Sample n1, treated at 200 °C, displays a coercivity (Hc) of 162.83 G, while sample n2, treated at 400 °C, shows a slightly higher coercivity of 173.66 G. These relatively elevated higher coercivity values indicate that neither sample exhibits clear superparamagnetic behavior. Superparamagnetic materials typically demonstrate very low coercivity values, indicating a propensity to rapidly respond to magnetic fields. The results imply that both n1 and n2 samples possess a certain resistance to demagnetization, hinting at enhanced magnetic stability despite not displaying superparamagnetic characteristics.

The magnetic properties of materials can be influenced by various factors, including morphology, particle size, preparation method, and crystal structure[32,33]. These factors may have an impact on the NPs magnetic behavior by influencing the moments within them and the magnetic interactions between them. An understanding of the synthesized samples possible uses in industries like magnetic storage, magnetic resonance imaging (MRI), and magnetic sensing can be gained from their magnetic characterization. For magnetic materials to be tailored and perform optimally in a variety of technological applications, it is essential to comprehend their magnetic properties and how they depend on various parameters.

ZFC analysis

The Zero-field cooling (ZFC) curves of FeONPs are shown in Fig. 7. The sample n1 was prepared at 200 °C for 18 h, and sample n2 was prepared at 400 °C for 18 h. A SQUID magnetometer was used to record the ZFC curves. Samples n1 and n2 ZFC curves show that 304 *K* is the blocking temperature. This temperature is thought to be the threshold where thermal energy is enough to displace the magnetic interactions within the NPs. Consequently, the samples magnetic behavior might alter. At 304 *K* and 320 *K*, respectively, the magnetization curves for the two samples exhibit a steady upward trend with increasing temperature. This suggests that, even at room temperature, superparamagnetic properties exist. The growing magnetization indicates that as temperature rises, the NPs show greater alignment of their magnetic moments. More information and an analysis of the ZFC curves and their significance for the magnetic characteristics of the FeONPs can probably be found in the reference[34]. Upon comparing the magnetic properties of this work with those of previously synthesized FeONPs

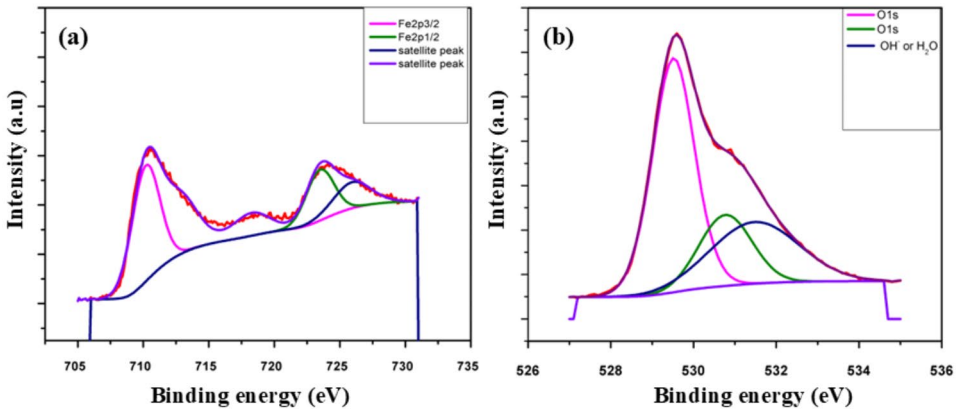

Fig. 5. XPS spectrum of (**a**) Fe2p, (**b**) O1s in FeONPs.

using microemulsion and alternative methods, it was found that the NPs produced by microemulsion had good coercivity and magnetic saturation, as shown in Table 4.

Conclusion

In this study, FeONPs with varying sizes, phases, and morphologies were successfully synthesized using the micro emulsion-hydrothermal approach, emphasizing the versatility of the method. The results reveal that synthesis temperature significantly impacted the shape of the nanoparticles, allowing for precise control over their structural characteristics. By systematically adjusting these parameters, we achieved optimal conditions for synthesizing FeONPs. Interestingly, the FeONPs demonstrated superparamagnetic behavior when synthesized at 200 °C for 18 h and 400 °C for 18 h, illustrating that how specific conditions effect their magnetic properties. These findings underscore the critical role of temperature and time in determining both the morphological and magnetic properties of nanoparticles, providing valuable insight for tuning the nanoparticles properties got different applications.

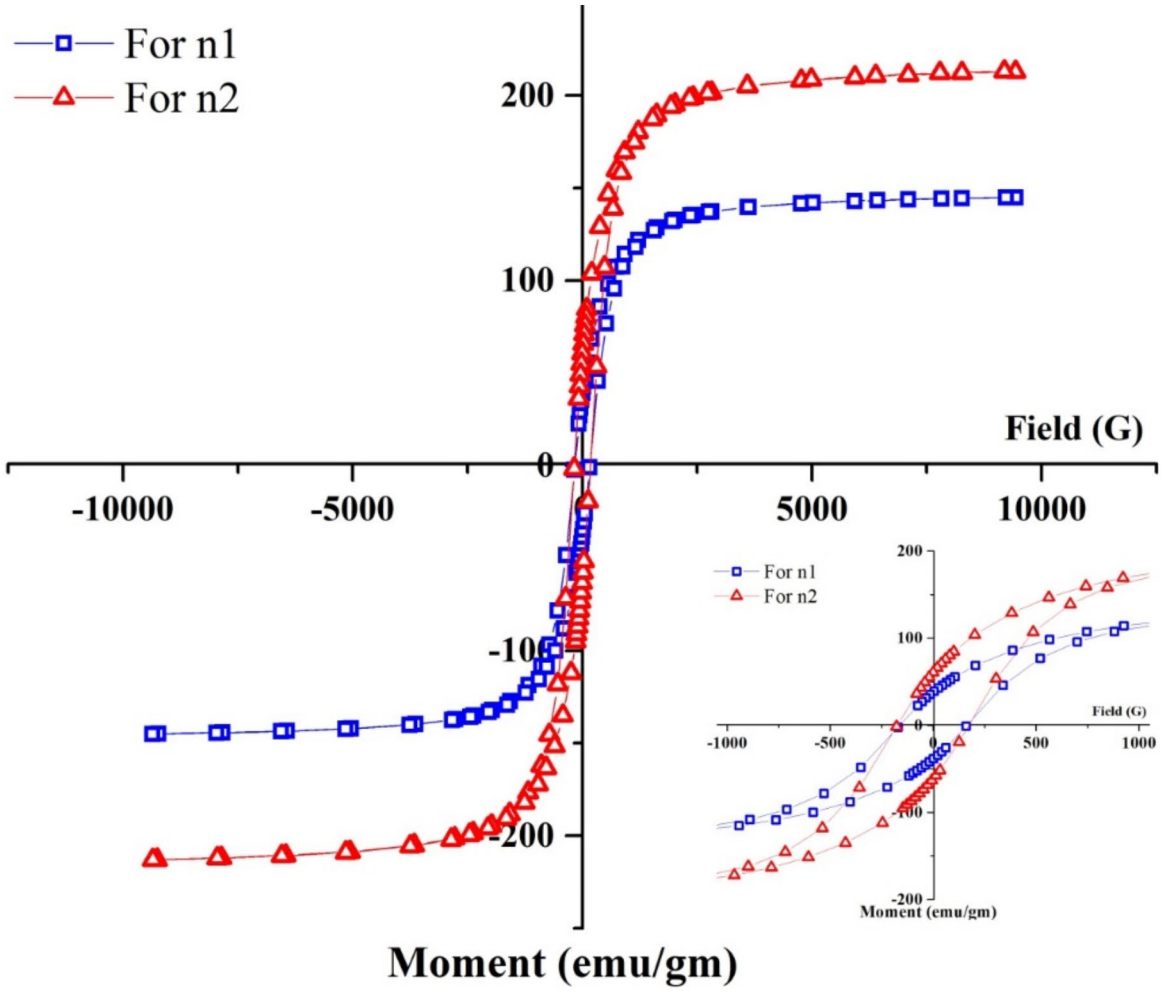

Fig. 6. Hhysteresis loops at room temperature for FeONPs synthesis by microemulsion- hydrothermal method (**a**) hematite (**b**) migmatite (**c**,**d**) magnetite.

Samples	Temp °C	Time (h)	Ms^{300k} [emu/g]	Mr^{300k} [emu/g]	Hc^{300k} [G]
n1	200		145.04	38.41	162.83
n2	400		213.11	60.98	173.66

Table 3. The magnetic properties of NPs synthesis by microemulsion- hydrothermal method.

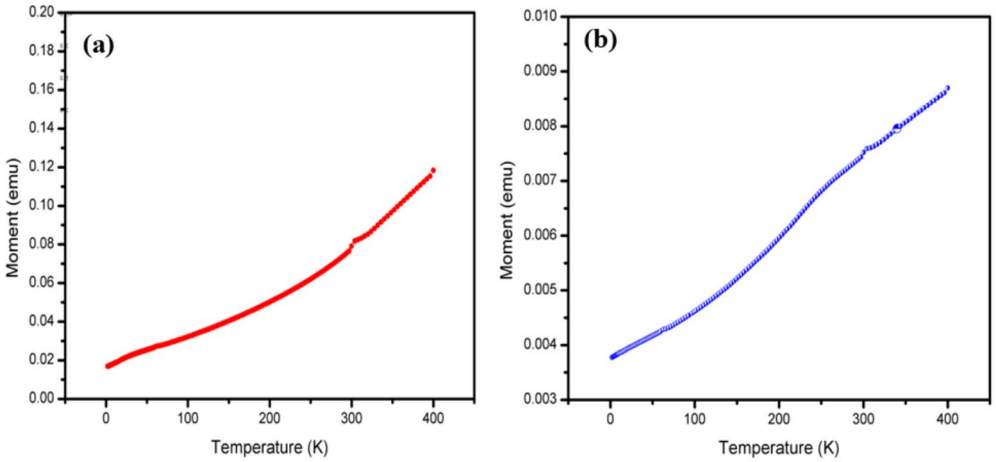

Fig. 7. ZFC of the as synthesized FeONPs under an applied field Oe (**a**) n1 and (**b**) n2.

Method	Precursor	Products	Ms (emu/g)	Hc Oe	Bt	Ref
Micro emulsion	$FeSO_4.nH_2O$	Fe_3O_4	18.3	–	–	22
Microemulsion	$FeCl_2.nH_2O$	Fe_3O_4	30	60	50 k	35
Hydrothermal	$FeCl_2.nH_2O$	Fe_3O_4	56	108	–	36
Microemulsion	$FeSO_4.7H_2O$	γFe_2O_3	37	–	–	37
Microemulsion	$FeSO_4.7H_2O$	γFe_2O_3	50	32	92	38
One-step perception	$Fe(CO)_5$	Fe_3O_4	12	117	–	39
Carbon reduction	Fe_2Cl_6	Fe_3O_4	34	40	–	40
Carbon reduction	$FeSO_4.7H_2O$	$Fe_3O_4@SiO_4$	46	21	–	41
This work	$Fe(NO_3)3.9H_2O$	Fe_3O_4	213	173	304	

Table 4. Comparison between the magnetic properties of the researchers work and reported research work (all at 300 k temperature).

Data availability

All the data is provided within the manuscript file.

Received: 17 October 2024; Accepted: 1 January 2025
Published online: 06 January 2025

References

1. Roy, S. D., Das, K. C. & Dhar, S. S. Conventional to green synthesis of magnetic iron oxide nanoparticles; its application as catalyst, photocatalyst and toxicity: a short review. *Inorg. Chem. Commun.* **134**, 109050 (2021).
2. Yang, C., Wu, J. & Hou, Y. Fe 3 O 4 nanostructures: synthesis, growth mechanism, properties and applications. *Chem. Commun.* **47**(18), 5130–5141 (2011).
3. Dey, A. et al. State of the art and prospects for halide perovskite nanocrystals. *ACS nano* **15**(7), 10775–10981 (2021).
4. Boles, M. A., Engel, M. & Talapin, D. V. Self-assembly of colloidal nanocrystals: from intricate structures to functional materials. *Chem. Rev.* **116**(18), 11220–11289 (2016).
5. Chen, Y. et al. Two-dimensional metal nanomaterials: synthesis, properties, and applications. *Chem. Rev.* **118**(13), 6409–6455 (2018).
6. Wu, L., Mendoza-Garcia, A., Li, Q. & Sun, S. Organic phase syntheses of magnetic nanoparticles and their applications. *Chem. Rev.* **116**(18), 10473–10512 (2016).
7. Uyama, T., Mukai, K. & Yamada, I. Facile and low-temperature synthesis of γ-Fe2O3 nanoparticles with thermally stable ferrimagnetism for use in magnetic recording tapes. *ACS Appl. Nano Mater.* **3**(11), 10678–10690 (2020).

8. Chin, A. B. & Yaacob, I. I. Synthesis and characterization of magnetic iron oxide nanoparticles via w/o microemulsion and Massart's procedure. *J. Mater. Process. Technol.* **191**(1–3), 235–237 (2007).
9. Biehl, P., Von der Lühe, M., Dutz, S. & Schacher, F. H. Synthesis, characterization, and applications of magnetic nanoparticles featuring polyzwitterionic coatings. *Polymers* **10**(1), 91 (2018).
10. Xi, G., Wang, C. & Wang, X. *The Oriented Self-Assembly of Magnetic Fe3O4 Nanoparticles into Monodisperse Microspheres and Their Use as Substrates in the Formation of Fe3O4 Nanorods* (Wiley Online Library, 2008).
11. Palanisamy, S. & Wang, Y. M. Superparamagnetic iron oxide nanoparticulate system: synthesis, targeting, drug delivery and therapy in cancer. *Dalton Trans.* **48**(26), 9490–9515 (2019).
12. Zhao, S. et al. Multifunctional magnetic iron oxide nanoparticles: an advanced platform for cancer theranostics. *Theranostics* **10**(14), 6278 (2020).
13. Lu, T. et al. Surfactant effects on the microstructures of Fe3O4 nanoparticles synthesized by microemulsion method. *Colloids Surf., a* **436**, 675–683 (2013).
14. Aisida, S. O. et al. Biogenic synthesis enhanced structural, morphological, magnetic and optical properties of zinc ferrite nanoparticles for moderate hyperthermia applications. *J. Nanopart. Res.* **23**, 1–14 (2021).
15. Rajapantulu, A. & Bandyopadhyaya, R. Formation of gold nanoparticles in water-in-oil microemulsions: experiment, mechanism, and simulation. *Langmuir* **37**(22), 6623–6631 (2021).
16. Rahaman, S. M. et al. A pH switchable Pickering emulsion stabilised by controlled non-conventional lanthanum sulfide nanoparticles, in situ hydrophobized with a cationic surfactant. *New J. Chem.* **48**(9), 4063–4076 (2024).
17. Chaudhary, R. G. et al. Metal/metal oxide nanoparticles: toxicity, applications, and future prospects. *Curr. Pharm. Design* **25**(37), 4013–4029 (2019).
18. Pavoni, L. et al. An overview of micro-and nanoemulsions as vehicles for essential oils: Formulation, preparation and stability. *Nanomaterials* **10**(1), 135 (2020).
19. Mathew, D. S. & Juang, R. S. An overview of the structure and magnetism of spinel ferrite nanoparticles and their synthesis in microemulsions. *Chem. Eng. J.* **129**(1–3), 51–65 (2007).
20. Tartaro, G. et al. Microemulsion microstructure (s): a tutorial review. *Nanomaterials* **10**(9), 1657 (2020).
21. Pang, Y. L., Lim, S., Ong, H. C. & Chong, W. T. Research progress on iron oxide-based magnetic materials: synthesis techniques and photocatalytic applications. *Ceram. Int.* **42**(1), 9–34 (2016).
22. Gradzielski, M. et al. Using microemulsions: formulation based on knowledge of their mesostructure. *Chem. Rev.* **121**(10), 5671–5740 (2021).
23. Samrot, A. V. et al. A review on synthesis, characterization and potential biological applications of superparamagnetic iron oxide nanoparticles. *Curr. Res. Green. Sustainable Chem.* **4**, 100042 (2021).
24. Okoli, C. et al. Comparison and functionalization study of microemulsion-prepared magnetic iron oxide nanoparticles. *Langmuir* **28**(22), 8479–8485 (2012).
25. Vidal-Vidal, J., Rivas, J. & López-Quintela, M. Synthesis of monodisperse maghemite nanoparticles by the microemulsion method. *Colloids Surf., A* **288**(1–3), 44–51 (2006).
26. Justus, J. S., Roy, S. D. D., Saravanakumar, K. & Raj, A. M. E. Judging phase purity of hematite (α-Fe2O3) nanoparticles through structural and magnetic studies. *Mater. Res. Express* **8**(5), 055005 (2021).
27. Chirita, M. et al. *Synthesis of micrometric single crystalline magnetite with superparamagnetic properties for biomedical applications*. In *NSTI-Nanotech* (2013).
28. Suppiah, D. D., Abd, S. B. & Hamid One step facile synthesis of ferromagnetic magnetite nanoparticles. *J. Magn. Magn. Mater.* **414**, 204–208 (2016).
29. Justus, J. S., Roy, S. D. D., Raj, A. M. E. & Bououdina, M. The role of pH and effect of calcination temperature on polymorphs and properties of iron oxide nanoparticles. *Int. J. Nanopart.* **11**(1), 62–78 (2019).
30. Pandey, S. et al. Locust Bean gum-based hydrogels embedded magnetic iron oxide nanoparticles nanocomposite: Advanced materials for environmental and energy applications. *Environ. Res.* **214**, 114000 (2022).
31. Kesse, X. et al. Elaboration of superparamagnetic and bioactive multicore–shell nanoparticles (Γ-Fe2O3@ SiO2-CaO): a promising material for bone cancer treatment. *ACS Appl. Mater. Interfaces* **12**(42), 47820–47830 (2020).
32. Zhao, L. et al. Sandwich-structured graphene-Fe3O4@ carbon nanocomposites for high-performance lithium-ion batteries. *ACS Appl. Mater. Interfaces* **7**(18), 9709–9715 (2015).
33. Chang, F. et al. Np heterojunction Bi4O5I2/Fe3O4 composites with efficiently magnetic recyclability and enhanced visible-light-driven photocatalytic performance. *Sep. Purif. Technol.* **238**, 116442 (2020).
34. Ajinkya, N. et al. Magnetic iron oxide nanoparticle (IONP) synthesis to applications: present and future. *Materials* **13**(20), 4644 (2020).
35. Samrot, A. & Sahithya, C. Selvarani A, SK Purayil and P. Ponnaiah. *Curr. Res. Green. Sustainable Chem.* **4**, 100042 (2021).
36. Cardoso, V. F. et al. Advances in magnetic nanoparticles for biomedical applications. *Adv. Healthc. Mater.* **7**(5), 1700845 (2018).
37. Osman, A. I. et al. Methods to prepare biosorbents and magnetic sorbents for water treatment: a review. *Environ. Chem. Lett.* **21**(4), 2337–2398 (2023).
38. Yazdani, F. & Seddigh, M. Magnetite nanoparticles synthesized by co-precipitation method: the effects of various iron anions on specifications. *Mater. Chem. Phys.* **184**, 318–323 (2016).
39. Zhou, X. et al. *Dispersing magnetic nanoparticles into staggered, porous Nano-Frameworks: weaving and visualizing Nanoscale magnetic flux lines for enhanced electromagnetic absorption*. *Adv. Funct. Mater.* 2314541 (2024).
40. Ma, Z. et al. Magnetic nanoparticles: synthesis, anisotropy, and applications. *Chem. Rev.* **123**(7), 3904–3943 (2021).
41. Kumar, S., Kumar, M., Velaga, S. & Singh, A. Tuneable optical properties of Fe2O3 magnetic nanoparticles synthesized from Ferritin. *J. Solgel Sci. Technol.* **105**(3), 650–661 (2023).

Acknowledgements

The research was funded by the Deanship of Scientific Research, Imam Mohammad Ibn Saud Islamic University (IMSIU), Saudi Arabia.

Author contributions

Shakeel Ahmad: Writing – review & editing, Software, Methodology, Investigation. Henmei Ni: Conceptualization, Project administration, Supervision, Writing – review & editing. Fahad S. Al-Mubaddel: Visualization, Software, Resources, Funding acquisition. Moustafa A. Rizk: Writing – review & editing, Software, Investigation, Data curation. Mohamed Ben Ammar: Data curation, Investigation, Writing – review & editing. Afaq Ullah Khan: Project administration, Methodology, Investigation, Conceptualization, Writing – review & editing, Supervision. Zainab M. Almarhoon: Data curation, Formal analysis, Visualization, Writing – review & editing. Abdulaziz A. Alanazi: Resources, Formal analysis, Data curation. Magdi E.A. Zaki: Writing – review & editing, Software, Resources, Investigation, Funding acquisition.

Declarations

Competing interests
The authors declare no competing interests.

Additional information
Correspondence and requests for materials should be addressed to H.N. or M.E.A.Z.

Reprints and permissions information is available at www.nature.com/reprints.

Publisher's note Springer Nature remains neutral with regard to jurisdictional claims in published maps and institutional affiliations.